Supplementary information
Inverse Hamiltonian design by automatic differentiation

Koji Inui and Yukitoshi Motome
Department of Applied Physics, The University of Tokyo, Hongo, Tokyo 113-8656, Japan

Supplementary Note 1: Rediscovery of the Haldane Model: initial condition dependence

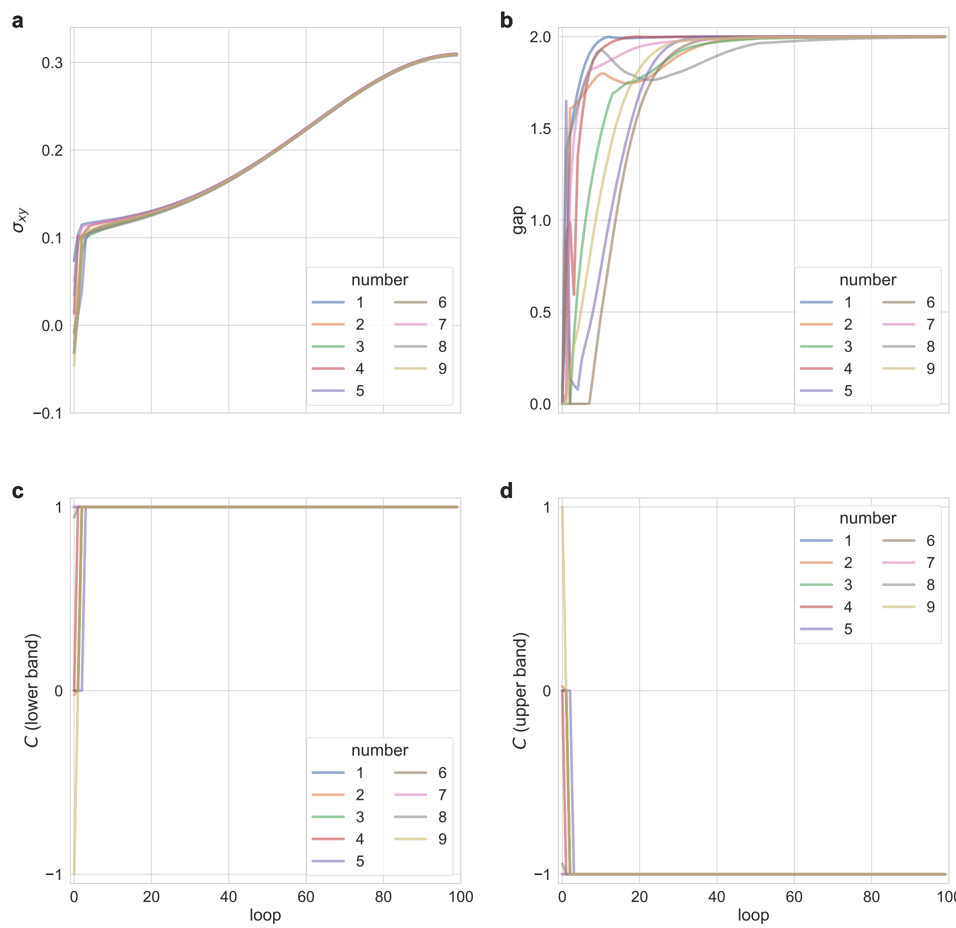

Supplementary Figure 1: Changes of the Hall conductivity σ_{xy} (**a**), the band gap (**b**), the Chern numbers of the lower band (**c**) and the upper band (**d**) for the tight-binding model on a honeycomb lattice in Eq. (1) in the main text. The number labels nine different sets of initial parameters.

Supplementary Figure 1 shows the optimization process of σ_{xy}, the band gap, and the Chern number of each band for nine sets of different initial parameters of the Hamitonian in Eq. (1) in the main text. All the cases converge to the same results. The changes of the model parameters are shown in Supplementary Figure 2. All of them converge to the same results corresponding to the center of the $C = 1$ phase of the Haldane model indicated by the star in Fig. 2**b** in the main text.

Supplementary Note 2: Discovery of a new Hamiltonian on a triangular lattice

A. Band structure

Supplementary Figure 3 shows the energy dispersion of each band for one of the optimal solution shown in Fig. 3**e** in the main text. The results indicate that the threefold rotational symmetry is approximately restored by the automatic optimization of σ_{xy}.

B. Initial condition dependence

Supplementary Figure 4 shows the optimization process of σ_{xy} for eighteen sets of different initial parameters of the Hamitonian on a triangular lattice in the main text. σ_{xy} converges to three different values; the largest one takes the value around 3.2, while the rest two are around 2.5 and 2.4.

C				Number of
1st	2nd	3rd	4th	initial conditions
5	1	-3	-3	10
3	3	-1	-5	3
3	2	-2	-3	2
3	1	-1	-3	3

Supplementary Table I: The Chern numbers of the four bands after the convergence starting from the eighteen different sets of initial parameters. The number of the initial conditions that converge to each result is also shown.

Supplementary Table I shows the Chern numbers of the four bands obtained from the different initial parameters. The number of the initial conditions that converge to the corresponding result is also listed. The majority is the group with $C = 5$, 1, -3, and -3, which gives $\sigma_{xy} \simeq 3.2$ in Supplementary Figure 4: ten out of eighteen initial conditions converge to this result, and one of them is discussed in the main text. Meanwhile, the group with $C = 3$, 3, -1, and -5 (three out of eighteen) also gives $\sigma_{xy} \simeq 3.2$ as the sum of C for the filled two bands are the same as the majority group. The rest two groups give the smaller $\sigma_{xy} \simeq 2.5$ and 2.4 in Supplementary Figure 4. Note that the four groups give $\sigma_{xy} = 6$, 6, 5, and 4 at zero temperature, corresponding to the sum of C for the filled two bands.

C. Refinement of the model parameters

As discussed in the main text, the phases of the hopping coefficients converge to rather scattered values. We find, however, that it is possible to regularize the parameters by hand while keeping the value of σ_{xy} by the following procedures. First, we set $|t_1| = |t_2| = |t_3| = 1$ and transform the hopping coefficients so as to shift the band bottom of the 1st band around $\boldsymbol{k}_0 = (\pi/2, \pi/(2\sqrt{3}))$ to the Γ point as $\tilde{t}_m^{ij} = t_m^{ij} \exp(\mathrm{i}\boldsymbol{d}^{ij} \cdot \boldsymbol{k}_0)$, where $\boldsymbol{d}^{ij}$ is a vector from site i to j in real space. Next, we set the phase of each hopping to a multiple of $\pi/4$ close to the value after the transformation. In addition, we tune a few of them by hand so as to make Φ_m spatially uniform. Then, we obtain the phases shown in Supplementary Figure 5**a**. These procedures provide us a Hamiltonian with regularized hopping coefficients, which looks similar to Fig. 3**f** in the main text but has spatially uniform fictitious magnetic fluxes as shown in Supplementary Figure 5**b**. This demonstrates that our framework is useful for constructing a new Hamiltonian in a regularized form.

Supplementary Note 3: Application to the photovoltaic effect: initial condition dependence

Supplementary Figure 6 shows the optimization process of the photocurrent I for nine sets of different initial parameters of the spin-charge coupled model in Eq. (2) in the main text. After the convergence, the results are grouped roughly into three; one of them gives the largest $I \sim 700$ Am^{-2}, as discussed in the main text.

Supplementary Table II shows the values of I, t_1, t_2, and J after the convergence starting from the different initial parameters. Three out of nine solutions converge to the largest value of $I \sim 700$ A/m^2. Spin configurations after the convergence are shown in Supplementary Figure 7. The results with the optimal value of I (number 3, 5, and 9) have an umbrella-shaped structure with three-site period. The others show different noncoplanar spin configurations.

number	J [eV]	t_1 [eV]	t_2 [eV]	I [A/m^2]
1	1.401	-0.054	-0.131	90
2	0.704	0.046	0.134	410
3	**0.279**	**-0.118**	**0.077**	**695**
4	0.770	0.122	0.071	263
5	**0.279**	**-0.118**	**0.077**	**695**
6	1.633	-0.036	0.137	30
7	1.398	0.051	0.132	87
8	0.379	0.063	0.127	605
9	**0.301**	**-0.119**	**-0.077**	**689**

Supplementary Table II: The values of J, t_1, t_2, and I for the different initial parameters after the convergence. The bold numbers indicate the results categorized into the optimal solution.

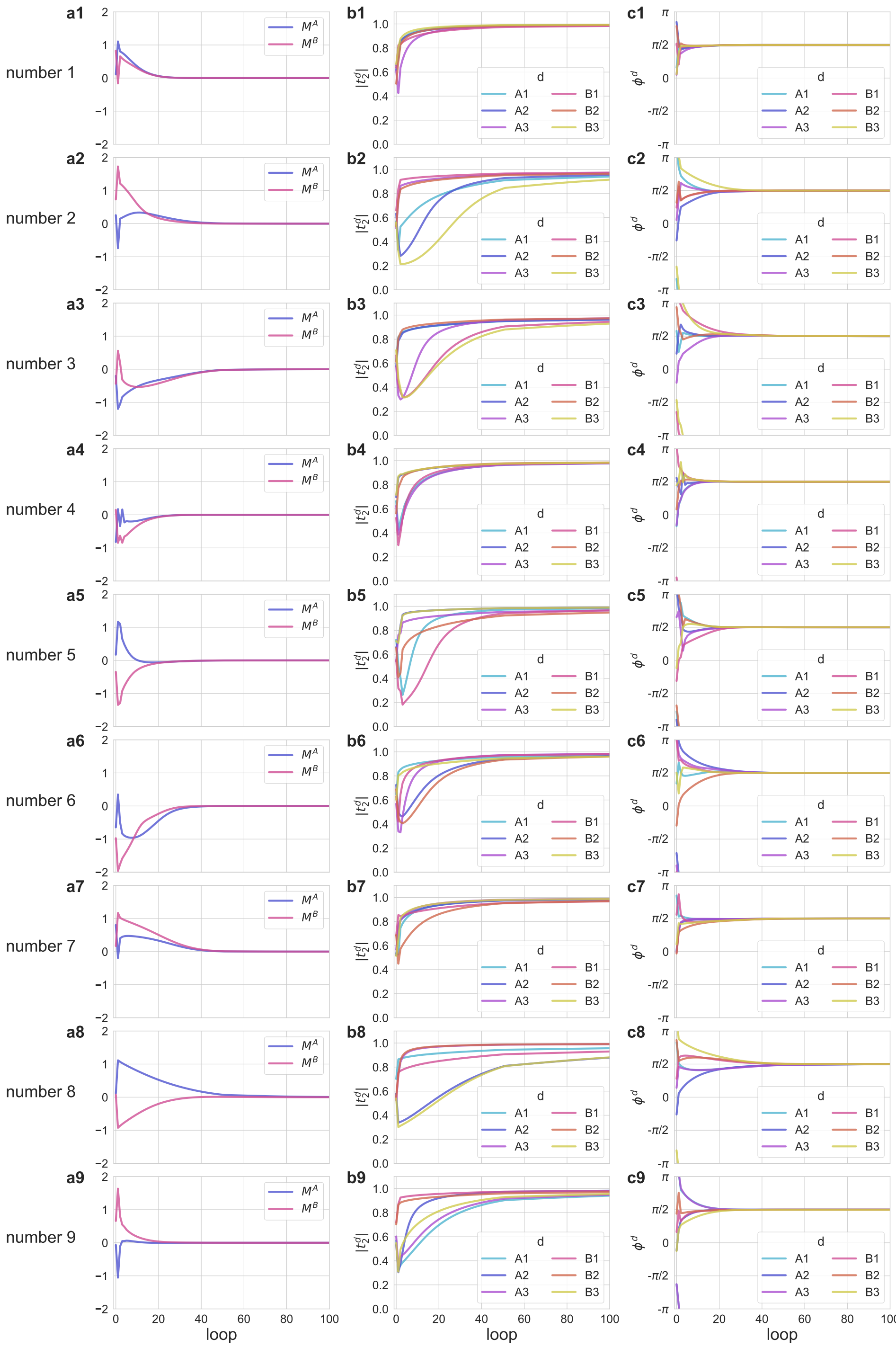

Supplementary Figure 2: Changes of M^{a_i} (**a1-9**), $|t_2^{d_{ij}}|$ (**b1-9**) and $\phi^{d_{ij}}$ (**c1-9**) for the tight-binding model on a honeycomb lattice in Eq. (1) in the main text for the nine sets of initial parameters.

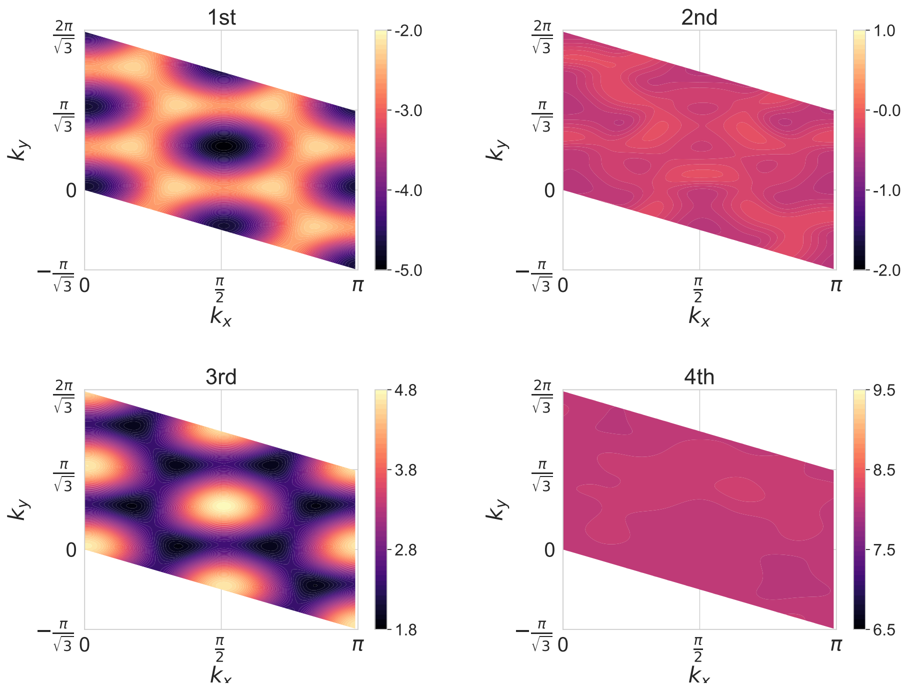

Supplementary Figure 3: The band structure after the convergence for the tight-binding model on a triangular lattice in the main text. All the bands restore approximately threefold rotational symmetry, while it is not so obvious for the 2nd and 4th bands since they are almost flat.

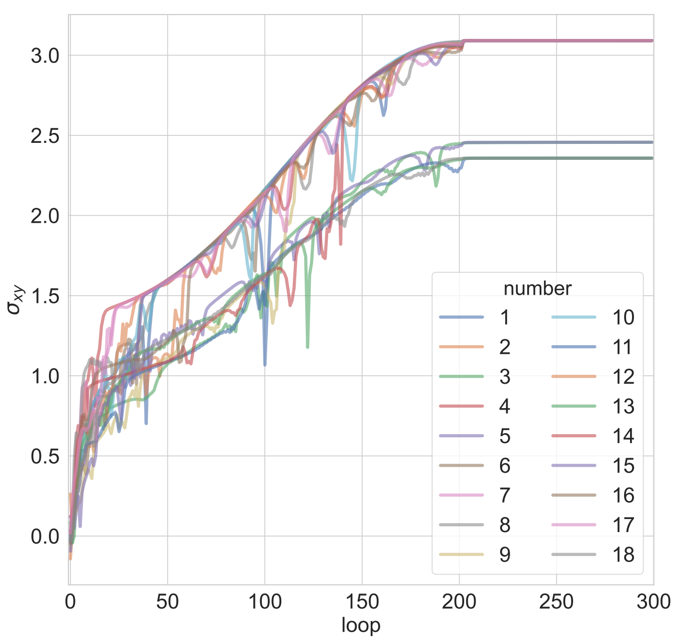

Supplementary Figure 4: Changes of the Hall conductivity σ_{xy} for the tight-binding model on a triangular lattice in the main text. The number labels eighteen different sets of initial parameters.

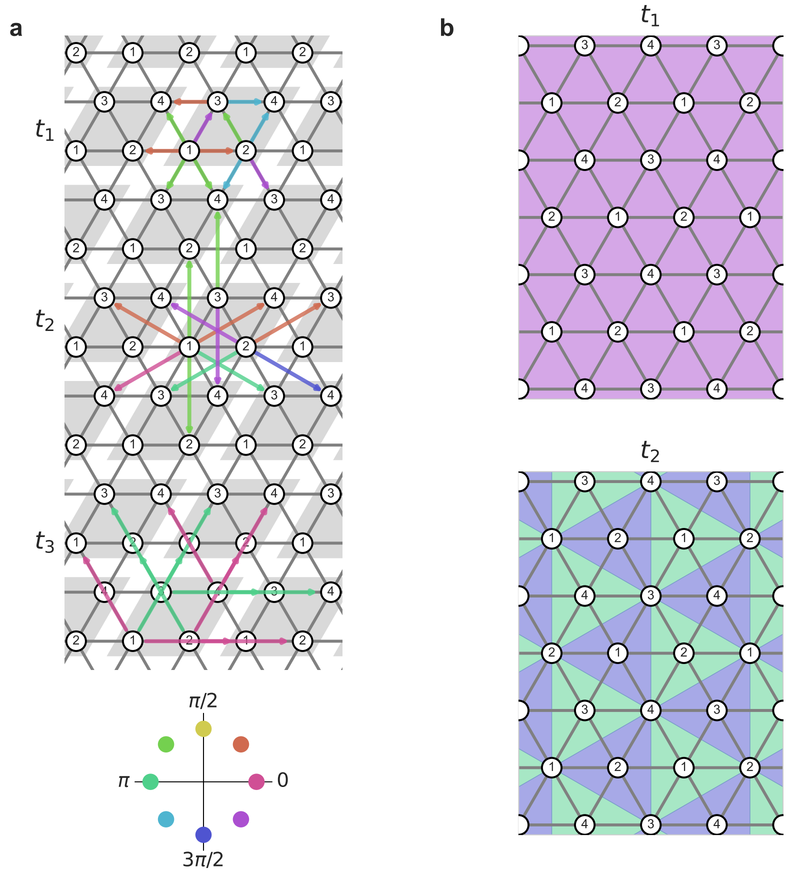

Supplementary Figure 5: **a**, The phases of the hopping coefficients of the tight-binding Hamiltonian on a triangular lattice after the refinement. All the phases are set to be multiples of $\pi/4$, as represented by the color of the arrows. The amplitudes of the hopping are taken as $|t_1| = |t_2| = |t_3| = 1$. **b**, Sum of the phases Φ_m defined in the main text for the triangles composed of t_1 (top) and t_2 (bottom).

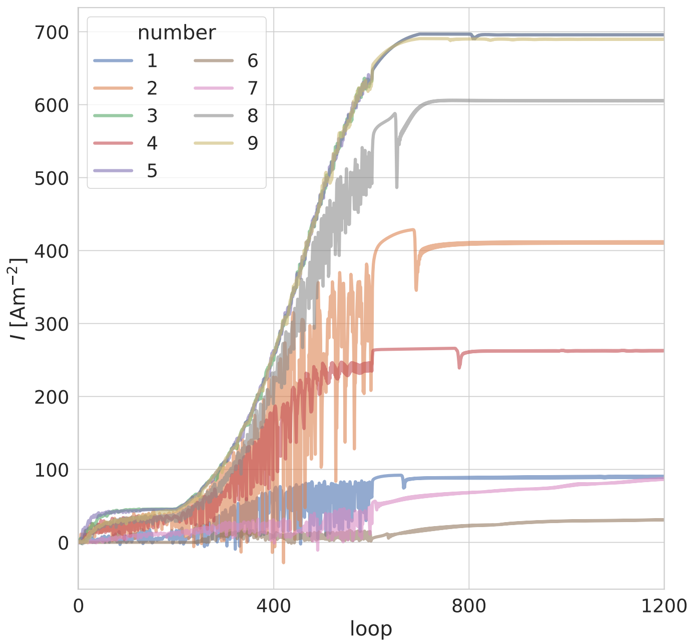

Supplementary Figure 6: Changes of the photocurrent through the optimization process for nine sets of different initial parameters.

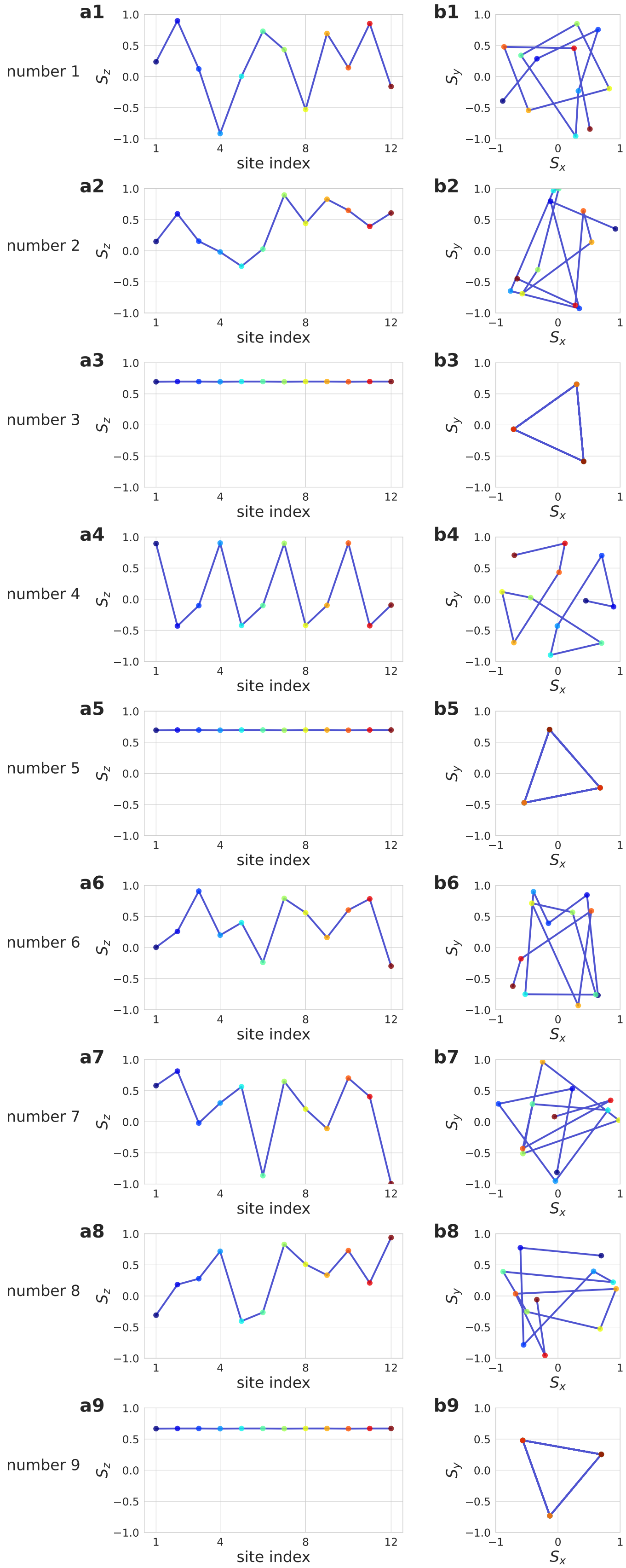

Supplementary Figure 7: Spin configurations for the different initial parameters: the z component, S_z (**a1-9**), and the xy components, S_x and S_y (**b1-9**). The S_z axis is taken in the direction of the total magnetization. The symbol color represents the site index.